Therapeutic Interfering Particles Exploiting Viral Replication and Assembly Mechanisms Show Promising Performance: A Modelling Study

Farzad Fatehi[1,2,+], Richard J. Bingham[1,2,3,+], Pierre-Philippe Dechant[1,2,4,+], Peter G. Stockley[5,*], and Reidun Twarock[1,2,3,*]

[1]**York Cross-disciplinary Centre for Systems Analysis, University of York, York YO10 5GE, UK**
[2]**Department of Mathematics, University of York, York YO10 5DD, UK**
[3]**Department of Biology, University of York, York YO10 5DD, UK**
[4]**School of Science, Technology & Health, York St John University, York YO31 7EX, UK**
[5]**Astbury Centre for Structural Molecular Biology, University of Leeds, Leeds LS2 9JT, UK**
[*]**corresponding authors: p.g.stockley@leeds.ac.uk (PGS) and rt507@york.ac.uk (RT)**
[+]**these authors contributed equally to this work**

ABSTRACT

Defective interfering particles arise spontaneously during a viral infection as mutants lacking essential parts of the viral genome. Their ability to replicate in the presence of the wild-type (WT) virus (at the expense of viable viral particles) is mimicked and exploited by therapeutic interfering particles. We propose a strategy for the design of therapeutic interfering RNAs (tiRNAs) against positive-sense single-stranded RNA viruses that assemble via packaging signal-mediated assembly. These tiRNAs contain both an optimised version of the virus assembly manual that is encoded by multiple dispersed RNA packaging signals and a replication signal for viral polymerase, but otherwise lack any genetic information. We use an intracellular model for hepatitis C viral (HCV) infection that captures key aspects of the competition dynamics between tiRNAs and viral genomes for virally produced capsid protein and polymerase. We show that only a small increase in the assembly and replication efficiency of the tiRNAs compared with WT virus is required in order to achieve a treatment efficacy greater than 99%. This demonstrates that the proposed tiRNA design could be a promising treatment option for RNA viral infections.

1 INTRODUCTION

Viruses are a major burden for public health and economy, yet our repertoire of antiviral options is still very limited. This is, in part, due to the high frequency with which viral genomes mutate and thus evade treatment. On the other hand, these mutations can sometimes lead to the production of defective viral genomes (DVGs) which are shed in defective interfering particles (DIPs). DVGs are spontaneously occurring mutants in a viral infection that lack essential genetic information, e.g. through deletion mutations, but are capable of replicating in the presence of, and indeed at the expense of, resources produced by viruses [25]. Many DVGs are well-known to have a replicative advantage over WT and to play a role in interference with WT virus [28], virus persistence [31] as well as specific [15] and unspecific immune activation [31, 38]. The exploitation of DIPs is a promising recent approach for therapy [15, 41, 50]. DIPs are selected and amplified for therapeutic use facilitated by advanced cloning techniques [15, 16, 32, 20, 30, 33], and have progressed to clinical stage [16, 14, 13, 12].

We propose here a novel strategy that exploits our discovery of packaging signal (PS)-mediated assembly in single-stranded RNA (ssRNA) viruses for the design of therapeutic interfering particles (TIPs) that mimick essential features of these DIPs. The genomes of many RNA viruses, including bacteriophages, plant viruses, and human pathogens present multiple dispersed sequence/structure motifs (PSs) with affinity for coat protein (Cp), which are embedded into their genetic message and collectively

promote virus assembly [45, 18, 46, 42, 35, 44, 43] (Fig. 1a). This is because they enable the virus to overcome the equivalent of Levinthal's Paradox in protein folding by biasing assembly towards a subset of energetically favourable pathways among the plethora of geometrically possible ones, which would require a much longer time to explore [19]. In some cases, such as in the Picornavirus human parechoviruses (HPeV), the PSs and their Cp binding sites have been characterised to atomistic detail [43]. They have also been identified in hepatitis B virus [35, 21], a DNA virus that packages its genome into its capsid in the form of pre-genomic RNA.

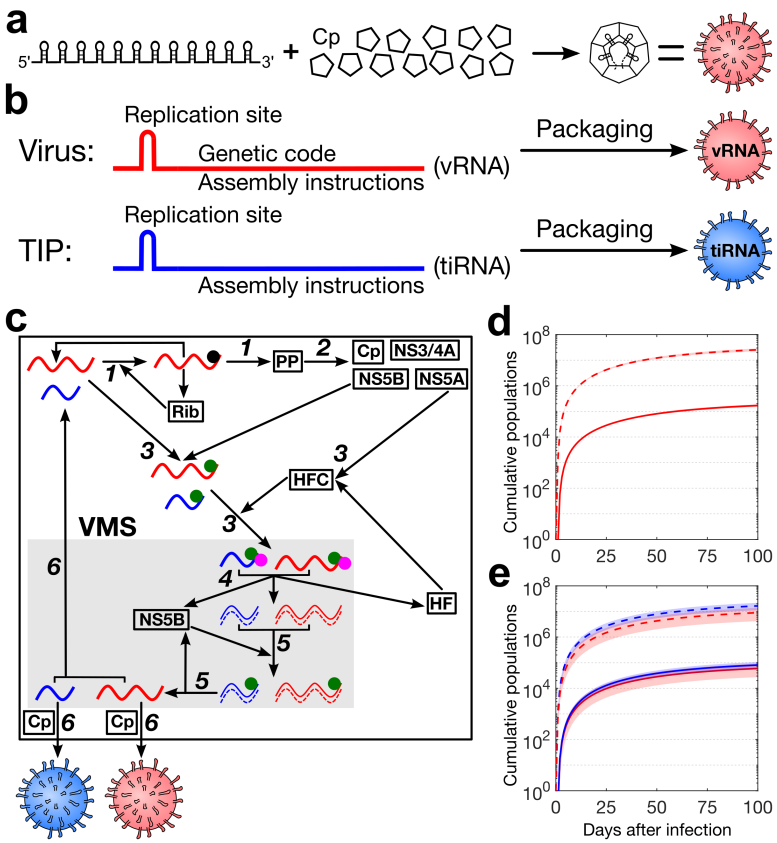

Figure 1. Assembly and intracellular dynamics of vRNAs and tiRNAs. (a) The PS-mediated assembly paradigm: Multiple sequence/structure motifs called packaging signals (PSs), that are dispersed throughout the viral genome, promote virion assembly via sequence specific interactions with coat protein (Cp). (b) vRNA and tiRNA in comparison: tiRNA is similar to vRNA but is devoid of any genetic message. (c) Schematic representation of the mathematical model for vRNA (red) and tiRNA (blue) in an HCV infection: In *step 1* and *2*; vRNA in the cytoplasm binds to free ribosomes to form a translation complex, which synthesizes the viral polyprotein (PP). The latter is cleaved, leading to the production of structural proteins such as core protein (Cp) and nonstructural proteins, including NS3/4A, NS5A, and NS5B. In *step 3*; NS5B and NS5A bind to vRNA or tiRNA and host factor (HF), respectively. These two complexes are imported into the vesicular membranous structure (VMS). In *step4*; the imported RNAs form double-strand RNAs (dsRNAs) and release NS5B and HF. In *step 5*; dsRNAs again bind to the NS5B and synthesise new vRNAs and tiRNAs. In *step 6*; these RNAs are either exported into the cytoplasm, or assembled into virions with 180 Cp and exported from the cell. (d) The time evolution of the HCV infection model shows the cumulative number of released virions (solid red line) and total vRNA (dashed red line), averaged over 250 simulations with the initial condition (+)RNA^{cyt}=1 and Cp=180. (e) The dynamics of virions and TIPs, where the solid red and blue lines indicate the released virions and TIPs, respectively, and the dashed red and blue lines the total vRNAs and tiRNAs, respectively, with the initial condition (+)RNA^{cyt}=1, (+)tiRNA^{cyt}=1 and Cp=360. The shaded areas highlight the regions of one standard deviation (std) from the mean. (d) and (e) are plotted using parameter values from Table 1 with $b_a = 1$ and $b_r = 1$.

Our detailed mechanistic understanding of PS-mediated assembly has enabled us to optimise the assembly code in satellite tobacco necrosis virus (STNV), creating RNA mutants that outcompete viral genomes in a competition assay [36]. Many of the best-studied examples of DVGs are found in (-)ssRNA viruses, which are presently known not assemble via multiple dispersed PSs. For viruses assembling via multiple dispersed PSs, indeed DIPs that are assembly competent and competitive with WT may not spontaneously arise through the standard mechanisms [31]; however, using our new mechanistic understanding they could be engineered. Here we propose to decouple the assembly code from the genetic message, and create synthetic assembly substrates containing only the PS-encoded virus assembly instructions allowing them to be efficiently encapsulated by viral Cp. To mimic the naturally occurring DIPs, we also include a recognition signal for viral replicase into these therapeutic interfering RNAs (tiRNAs), so that they are replicated by viral replicase (Fig. 1b), but no internal ribosome entry site (IRES), giving tiRNAs another competitive advantage by not spending time on translation.

Mathematical models of a viral infection can be used to assess the merits of novel antiviral strategies [21, 2]. The population dynamics of DIPs interacting with WT virus (called the 'helper' or 'standard' virus) can be complicated [26, 5, 47, 48] with chaotic or predator-prey dynamics, but often the parasitic relationship between DIPs and helper virus results in the attenuation or clearance of the original infection. Thus, we use HCV (an ssRNA virus) as a model system and we develop an extension of an intracellular model of HCV presented by Aunins *et al.* [4] that now includes also the dynamic competition between tiRNAs and viral RNAs (vRNAs).

2 RESULTS

2.1 Intracellular modelling of HCV infection and tiRNAs

Recently Aunins *et al.* presented a detailed, parameterised intracellular model for hepatitis C viral (HCV) infection based on experimental data [4]. The model consists of 6 steps (Fig. 1c). *Step 1*; positive-sense RNA strand in the cytoplasm [(+)RNA$^{\text{cyt}}$] binds to free ribosomes to form a translation complex (R:(+)RNA) at a rate k_{tc}, which synthesizes the viral polyprotein (PP) at a rate k_{trans}. *Step 2*; the cleavage of PPs at a rate $k_{cleavage}$ leads to production of structural proteins, including core protein (Cp) and nonstructural proteins, including NS3/4A, NS5A, and NS5B$^{\text{cyt}}$. *Step 3*; NS5B$^{\text{cyt}}$ (polymerase) and NS5A bind to (+)RNA$^{\text{cyt}}$ and host factor (HF) at rates k_{rp5b} and k_{hfc} to form NS5B:(+)RNA and HFC complexes, respectively. These two complexes are imported into the vesicular membranous structure (VMS) at a rate k_{rip} in a second-order reaction. *Step4*; the imported RNA forms a double-strand RNA (dsRNA) and releases NS5B$^{\text{VMS}}$ and HF at a rate k_{init}. *Step 5*; dsRNA binds to the NS5B$^{\text{VMS}}$ at a rate k_{rids} to synthesise (+)RNA$^{\text{VMS}}$ at a rate k_{repl}. *Step 6*; (+)RNA$^{\text{VMS}}$ in the VMS are either exported into the cytoplasm at a rate k_{outrp}, or assembled into virions with 180 Cp and exported from the cell at a rate $k_{assembly}$. The model was fitted to experimental data and estimated parameters values (Table 1)[4].

In this paper, we extend this model to include the dynamics of tiRNAs (Fig. 1c). Both the viral genome and tiRNA assemble via packaging signal (PS)-mediated assembly, i.e. both present PSs with affinity for viral Cp, ensuring efficient, specific genome packing. The PS distribution of the tiRNAs is optimised with respect to that of the virus, e.g. by stabilising key PSs in the distribution as in [36], enabling them to potentially assemble more efficiently than the virus (Fig. 1a). We consider tiRNAs which also contain the terminal sequences necessary for recognition by viral polymerases [15, 27, 29], so that they are replicated in the presence of the virus (Fig. 1b). As there is no protein coding requirement, and indeed no IRES, tiRNAs replication efficiency relative to the genome can be increased by shortening of the genome, or by tuning the nucleotide sequence [27, 29]. Thus, we model tiRNAs dynamics as follows: We assume that a positive-sense tiRNA in the cytoplasm [(+)tiRNA$^{\text{cyt}}$] binds to NS5B$^{\text{cyt}}$ and HFC at rates k_{rp5b} and k_{rip}, respectively, to be imported into the VMS. Then, similar to viral RNAs (vRNAs), they produce double-strand tiRNA and (+)tiRNA$^{\text{VMS}}$ at rates $b_r k_{init}$ and $b_r k_{repl}$, respectively, where b_r characterises the replication efficiency of the tiRNAs. A tiRNA with $b_r = 1$ would be transcribed at the same rate as vRNAs. The newly formed (+)tiRNA$^{\text{VMS}}$ is then either exported into the cytoplasm at a rate k_{outrp} or assembled into TIPs with 180 Cp and exported from the cell at a rate $b_a k_{assembly}$, where b_a characterises the assembly efficiency of the tiRNAs (Fig. 1c). The assembly efficiency of a tiRNA can be tuned by alteration of the PS distribution, for instance, a competition experiment between STNV and a copy with an optimised PS distribution resulted in encapsidation in a ratio of 1 : 2 to 1 : 3 [36], suggesting that $b_a \sim 2.5$ is experimentally achievable. The reactions of the model are provided in Methods.

Aunins *et al.*[4] used ordinary differential equations (ODE) to model the production of virions over a

relatively short timescale (50 hours). However, as we wish to model longer time periods, we implemented the model using discrete reaction networks, as solving ODEs for times longer than 200 hours was found to be not computationally feasible. As the average life span of adult hepatocytes ranges from 200 to 300 days [17] and half-life of infected cells by HCV is estimated to be from 1.4 to 700 days [10], we ran our simulations for 100 days, after which the qualitative outcomes for the cells is well established. Using discrete reaction networks will also enable tracking of particles at low concentrations during the kinetic phase.

2.2 Single cell viral dynamics

Here we study the viral dynamics in the absence and presence of tiRNAs. The dynamics are computed as an average over stochastic simulations of the reaction network using the Gillespie algorithm [23] implemented in Fortran and using parameter values from Table 1 and initially, with $b_a = 1$ and $b_r = 1$.

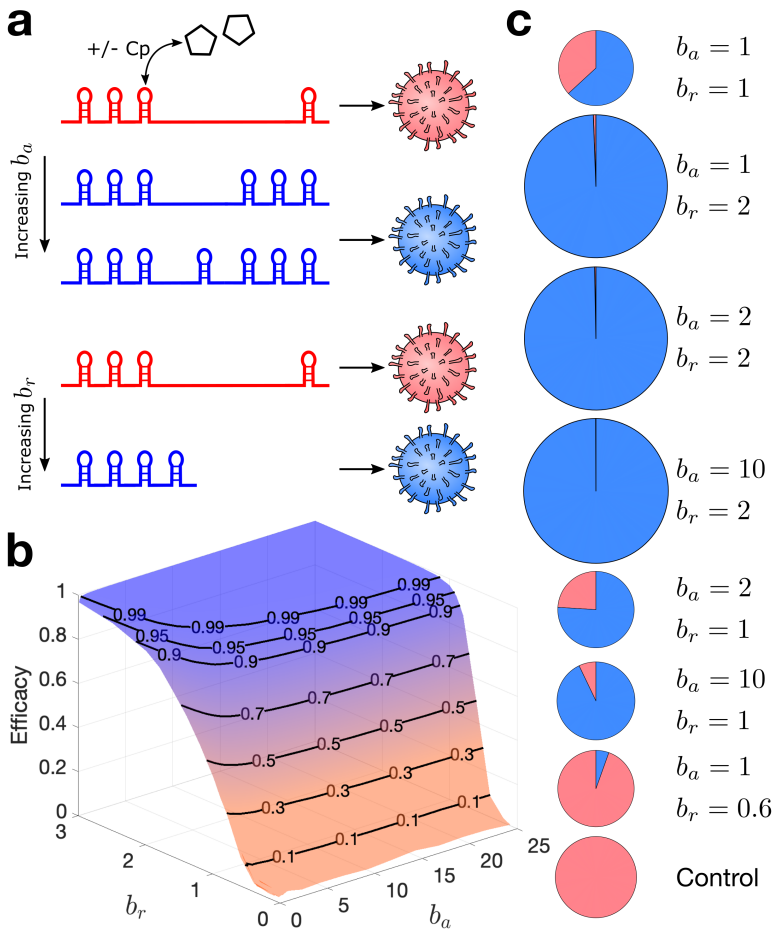

Figure 2. The impact of replication and assembly efficiencies on the treatment efficacy and cumulative number of released virus-like particles. (a) TIP design is defined by two parameters: assembly efficacy b_a, which can be changed by addition of PSs in the tiRNAs (blue) compared with vRNA (red), and replication efficacy b_r, which can be improved by shortening of tiRNA with respect to vRNA. (b) The efficacy of tiRNAs (shown as the fraction indicating reduction in the number of released infectious virions) as a function of b_a and b_r. (c) Pie charts for the cumulative number of released virions and TIPs after 100 days post infection. Red and blue indicate virions and TIPs, respectively. The tiRNA-free control is shown for comparison. The area of each graph is proportional to the total number of released particles (virion+TIP) with respect to the control. For $b_r \leq 1$ the total number of released particles is less than the control while for $b_r = 2$ the total number of released particles is 3 times of the control. (b) and (c) are plotted by averaging over 250 simulations with the initial condition (+)RNA^{cyt}=1, (+)tiRNA^{cyt}=1 and Cp=360, using parameter values from Table 1.

The multiplicity of infection (MOI) is set to one vRNA and one tiRNA, consistent with data for intranasal sprays for clonal influenza DIPs [15]. Figure 1d indicates the total number of released virions (solid red line) and vRNAs in the cell (dashed red line) in the absence of co-infecting tiRNAs. Figure 1e shows the effect on viral dynamics of introducing tiRNAs. Co-infection with tiRNAs reduces the level of released virions by 70% (this reduction is called the treatment efficacy), while the number of tiRNAs within the cell is comparable with the level of vRNAs in the tiRNA-free case. This shows that even without an advantage in replication or assembly, the lack of a protein-coding responsibility and IRES enables tiRNAs to displace vRNAs as the most frequently packaged contents of new virus-like particles (VLPs).

The impact of the tiRNAs relies on two characteristic features: their relative replication (b_r) and assembly (b_a) efficiency compared with helper virus. We therefore investigate the impact of these two descriptors on the infection dynamics.

2.3 The effect of replication and assembly efficiencies

tiRNAs assembly and replication efficiency can be increased by adding more PSs into the genome, stabilising PSs or increasing their binding affinity, and shortening of the genome respectively (Fig. 2a). Though many DVGs are well-known to have a replicative advantage over WT [31, 40, 41], the length of the genome is not the only factor that determines the replication efficiency (b_r) [49, 29]. Thus, we also consider the cases where $b_r < 1$, i.e., where tiRNAs replicate less efficiently than WT virus. Figure 2b indicates for $b_r < 0.7$ the efficacy of tiRNAs is below 50%, even for high values of b_a (assembly efficiency). This illustrates the importance of the replication process in the viral life cycle, as tiRNAs must be at least as efficient as WT virus at replication in order to be a viable treatment option. For $b_r \leq 1$, i.e. if tiRNAs are not more efficient at replication than virus, the total number of released particles is lower than the tiRNA-free control, while for $b_r > 1$ the total number of released particles increases, however this is overwhelmingly dominated by TIPs (Fig. 2c). This increase in the number of TIPs will increase the level of antigen and could have consequences for the immune response. However, increasing of b_a alone does not lead to an increase in the level of total released particles (Fig. 2c). Interestingly, the benefits of the treatment have a saturation point; increasing $b_a > 10$ and increasing $b_r > 2$ does not have a significant impact on the efficacy of the treatment and total number of released particles (Fig. 2b and c).

Even for $b_a = b_r = 1$, i.e. for equal replication and assembly efficiency as the virus, the number of released TIPs is higher than that of infectious virions. This is because tiRNAs have a competitive advantage over virus as they are depleting resources generated only by the virus, using virally generated polymerase for replication and Cp for assembly. In particular, during the time that vRNA is bound to ribosome, tiRNA is free to bind to NS5B and replicate at the expense of the virus, resulting in the inherent asymmetry between virus and TIP.

2.4 The effect of higher multiplicities of infection (MOIs)

The above results have been obtained in the equitable case of an MOI of 1:1. Experimental work on comparable systems have reported DIP MOIs in the range $1-100$ [15, 47, 1], therefore we should consider cases with unequal starting proportions of vRNA and tiRNA. We next determine the release kinetics for higher MOIs, setting $b_a = b_r = 1$ in order to isolate the effect of the MOI.

For MOIs of tiRNA (T) higher than the MOI of vRNA (V), the number of released virions decreases while increasing the ratio of TIPs/Virions (Fig. 3), with TIPs swiftly dominating the population. However, for MOIs of vRNA larger than the MOI of tiRNA, a much smaller effect occurs (Fig. 3) and virions outnumber the TIPs, demonstrating that the relative ratio of virus and TIPs is important for the outcome of the treatment. From Fig. 3 we can see that when the MOI of tiRNA and vRNA is equal V=T=1 the released particles are dominated by TIPs in a roughly 1.5:1 ratio with the virions. This suggests that in a population of infected cells, the subsequent infections would also be seeded by MOIs with more tiRNAs than vRNAs, moving rightward in Fig. 3, leading to a population of released particles dominated by non-infectious TIPs, potentially causing the elimination of the wider infection. A within-host model of the HCV in the presence of tiRNAs is required to fully examine this potential.

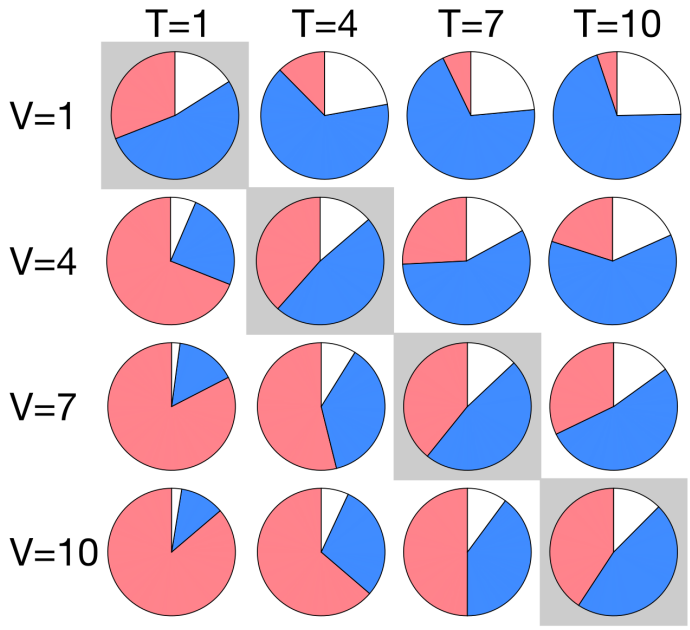

Figure 3. Increasing the MOI of tiRNA (T) increases the cumulative number of released TIPs and reduces the total number of released particles (virion+TIP) compared with the control. Pie charts for the cumulative number of released virions and TIPs after 100 days post infection. Red and blue indicate the number of virions and TIPs, respectively, while white shows the difference between the total number of released virions in the control (tiRNA-free) case with the number of released particles (virion+TIP) in the presence of treatment. This figure is plotted by averaging over 250 simulations using parameter values from Table 1 with $b_a = 1$ and $b_r = 1$. The initial condition for the MOIs of V=m, T=n is (+)RNA$^{\text{cyt}}$=m, (+)tiRNA$^{\text{cyt}}$=n, and Cp=180$(m+n)$.

2.5 The effect of treatment starting time

The results presented above are based on the assumption that both the vRNAs and the tiRNAs begin the infection at the same time, however this would not necessarily be the case *in vivo*. Figure 4 shows that if the MOI of tiRNA is larger than that of vRNA (blue shaded area) the efficacy is higher than the average efficacy (solid black line). On the other hand, while if the MOI of vRNA is larger than that of tiRNA (red shaded area) the efficacy is lower than the average efficacy. If each cell that is infected by a vRNA already harbours at least one tiRNA (start of treatment = 0 hour), we get the highest treatment efficacy (Fig. 4). However if treatment is started (i.e. the tiRNAs are introduced) 24 hours post infection, this treatment option has no significant effect on the outcome of the infection even if b_a, b_r are high and the MOI of tiRNAs is higher than the MOI of vRNAs (Fig. 4). This suggests that tiRNAs can be highly effective when used as a prophylactic antiviral treatment, an approach that has recently gained wider attention [15, 9]. Recent experiments for influenza DIPs have established that prophylactic intranasal treatment can achieve delivery of around one DIP per susceptible cell, where they can stay present for several weeks [15]. Although evaluation of the full impact of TIPs as a treatment option during a chronic infection needs to be studied in the context of a within-host model, our model provides the foundation for studying such aspects by coupling of the intracellular model presented here with an intercellular model in a multiscale approach [37, 22].

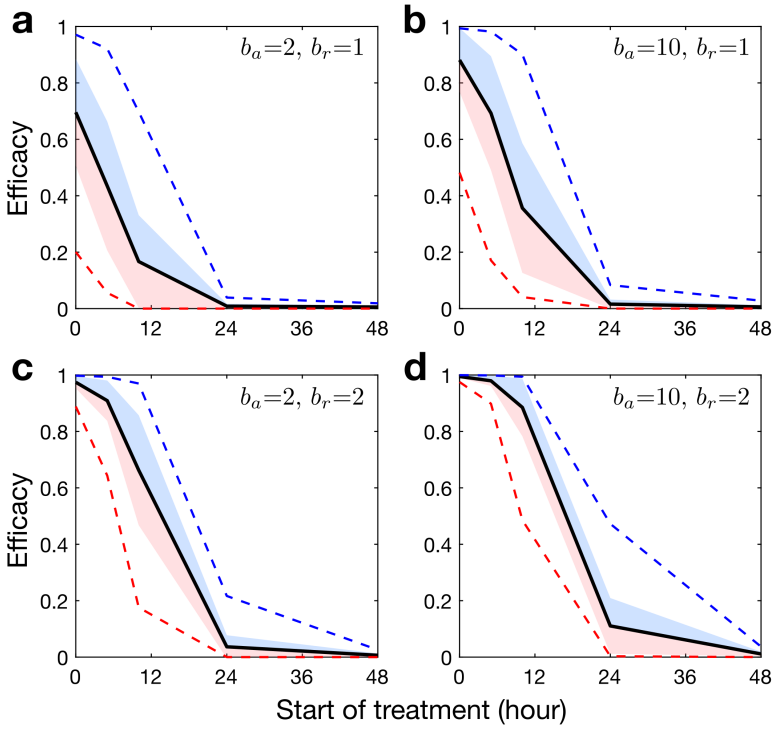

Figure 4. Starting treatment 24 hours after cell infection has no significant impact even for high replication and assembly efficiencies and MOIs. The black curves indicate the average of efficacy over varying MOI of vRNAs and tiRNAs from 1 to 10 ($1 \leq V \leq 10$, $1 \leq T \leq 10$). Blue and red shaded areas show the regions of mean+std and mean-std, respectively. Blue and red dashed lines indicates the maximum and minimum efficacy of treatment over various MOIs, respectively.

3 DISCUSSION

In this paper we have exploited recent insights into PS-mediated assembly in order to propose a novel design for TIPs that combines the replicative advantages of existing DIP/TIP strategies over viruses [39, 15, 32] with the benefits of PS-mediated assembly. This novel design for TIPs opens up unprecedented therapeutic potential to interfere with viral replication and assembly, and misdirect viral resources. We have demonstrated the benefits of this combined strategy through mathematical modelling.

The tiRNA designs proposed here are attractive alternatives to drugs directed against the PS:RNA contacts acting as decoys rather than inhibiting contact formation. Some viruses have been repurposed by nature for vital functions in the host organism. For instance, captured retroviruses and retrotransposons can be expressed in different tissues and at different points during life cycles, such as in neuronal functioning [34, 3] or placentation [24, 8, 7, 11]. Any PS-targeting drugs interfering with virus assembly would therefore have to be monitored carefully with regards to their effect on other vital functions. tiRNAs, on the other hand, would not pose that risk.

However, they have the same benefits as PS-targeting drugs from the point of view of viral escape. This is because in both cases, viral escape would require mutation of the full set (or a significant subset) of the PSs, which would result in a significant intermittent fitness loss due to the multiple dispersed nature of the PSs [6], making such a transition highly unlikely. The low propensity for therapy resistance is shared by other DIPs/TIPs, where resistant strains have been shown to be selected against at both individual and population level [39]. However, our tiRNA design has a distinct advantage over these other strategies: Being stripped of all genetic information, they do not pose the risk of recombination. This is in contrast with DIPs that arise via deletion of a portion of the viral sequence, such as one genomic segment in the case of the multi-segmented influenza virus [15], retaining the coding capacity for some of the gene products.

As we have shown, tiRNAs can be effective as a treatment, especially as a prophylactic treatment to prevent infection. We have also shown that producing a tiRNA needs to only be as effective at packaging

and replicating as vRNA to dominate the released particles. As TIPs are indistinguishable from virus at the particle exterior and increasing their replication efficacy leads to a high level of TIPs (increasing the level of antigen), they can elicit the immune response which could interfere with a subsequent infection, attenuating or clearing the infection. Thus, a further direction of study could develop multiscale within-host models of the immune response to study the impact of TIPs on the immune response and analyse their effects during a chronic infection. Furthermore, presenting models with infection dynamics between hosts in order to study such impacts of TIPs on a host population could be interesting as TIPs can be transmitted between hosts, and thus confer additional benefits to the host population. Such models will also enable any risks associated with the use of TIPs to be evaluated [26, 47, 39].

4 METHODS

4.1 The model

The first step is the production of polyprotein (PP) using the host cell ribosomes (Rib) from the (+)RNA in cytoplasm [(+)RNA$^{\text{cyt}}$]:

$$\begin{aligned}
&(+)\text{RNA}^{\text{cyt}} + \text{Rib} \xrightarrow{k_{tc}} \text{R:(+)RNA},\\
&\text{R:(+)RNA} \xrightarrow{k_{trans}} \text{PP} + \text{Rib} + (+)\text{RNA}^{\text{cyt}}.
\end{aligned}$$

Then, the viral proteins are cleaved in a single reaction from the PP:

$$\text{PP} \xrightarrow{k_{cleavage}} \text{Cp} + \text{NS3/4A} + \text{NS5A} + \text{NS5B}^{\text{cyt}}.$$

In the next step, NS5A and NS5B$^{\text{cyt}}$ bind to human factor (HF) and (+)RNA$^{\text{cyt}}$ or (+)tiRNA$^{\text{cyt}}$, respectively, and these two complexes are imported into the VMS in a second-order reaction:

$$\begin{aligned}
&(+)\text{RNA}^{\text{cyt}} + \text{NS5B}^{\text{cyt}} \xrightarrow{k_{rp5b}} \text{NS5B:(+)RNA},\\
&(+)\text{tiRNA}^{\text{cyt}} + \text{NS5B}^{\text{cyt}} \xrightarrow{k_{rp5b}} \text{NS5B:(+)tiRNA},\\
&\text{HF} + \text{NS5A} \xrightarrow{k_{hfc}} \text{HFC},\\
&\text{NS5B:(+)RNA} + \text{HFC} \xrightarrow{k_{rip}} \text{NS5B:(+)RNA:HFC},\\
&\text{NS5B:(+)tiRNA} + \text{HFC} \xrightarrow{k_{rip}} \text{NS5B:(+)tiRNA:HFC}.
\end{aligned}$$

The imported RNA (tiRNA) form a dsRNA (dstiRNA) and releases NS5B and HF:

$$\begin{aligned}
&\text{NS5B:(+)RNA:HFC} \xrightarrow{k_{init}} \text{NS5B}^{\text{VMS}} + \text{dsRNA} + \text{HF},\\
&\text{NS5B:(+)tiRNA:HFC} \xrightarrow{b_r k_{init}} \text{NS5B}^{\text{VMS}} + \text{dstiRNA} + \text{HF}.
\end{aligned}$$

Once again the dsRNA (dstiRNA) and NS5B$^{\text{VMS}}$ form a complex required to synthesise new (+)RNA$^{\text{VMS}}$ ((+)tiRNA$^{\text{VMS}}$):

$$\begin{aligned}
&\text{dsRNA} + \text{NS5B}^{\text{VMS}} \xrightarrow{k_{rids}} \text{NS5B:dsRNA},\\
&\text{dstiRNA} + \text{NS5B}^{\text{VMS}} \xrightarrow{k_{rids}} \text{NS5B:dstiRNA},\\
&\text{NS5B:dsRNA} \xrightarrow{k_{repl}} \text{dsRNA} + \text{NS5B}^{\text{VMS}} + (+)\text{RNA}^{\text{VMS}},\\
&\text{NS5B:dstiRNA} \xrightarrow{b_r k_{repl}} \text{dstiRNA} + \text{NS5B}^{\text{VMS}} + (+)\text{tiRNA}^{\text{VMS}}.
\end{aligned}$$

(+)RNA$^{\mathrm{VMS}}$ ((+)tiRNA$^{\mathrm{VMS}}$) either exported into the cytoplasm or assembled into new virions (TIPs) with Cp:

$$(+)\mathrm{RNA}^{\mathrm{VMS}} \xrightarrow{k_{outrp}} (+)\mathrm{RNA}^{\mathrm{cyt}},$$
$$(+)\mathrm{tiRNA}^{\mathrm{VMS}} \xrightarrow{k_{outrp}} (+)\mathrm{tiRNA}^{\mathrm{cyt}},$$
$$(+)\mathrm{RNA}^{\mathrm{VMS}} + 180\mathrm{Cp} \xrightarrow{k_{assembly}} \mathrm{virion},$$
$$(+)\mathrm{tiRNA}^{\mathrm{VMS}} + 180\mathrm{Cp} \xrightarrow{b_a k_{assembly}} \mathrm{TIP}.$$

Finally, we allow natural decay of vRNAs, tiRNAs, proteins and VMS via the reactions:

$$(+)\mathrm{RNA}^{\mathrm{cyt}} \xrightarrow{k_{degrp}} 0, \qquad (+)\mathrm{tiRNA}^{\mathrm{cyt}} \xrightarrow{k_{degrp}} 0,$$
$$\mathrm{NS5B{:}(+)RNA{:}HFC} \xrightarrow{k_{degvms}} 0, \qquad \mathrm{NS5B{:}(+)tiRNA{:}HFC} \xrightarrow{k_{degvms}} 0,$$
$$\mathrm{dsRNA} \xrightarrow{k_{degvms}} 0, \qquad \mathrm{dstiRNA} \xrightarrow{k_{degvms}} 0,$$
$$(+)\mathrm{RNA}^{\mathrm{VMS}} \xrightarrow{k_{degvms}} 0, \qquad (+)\mathrm{tiRNA}^{\mathrm{VMS}} \xrightarrow{k_{degvms}} 0,$$
$$\mathrm{NS5B{:}dsRNA} \xrightarrow{k_{degvms}} 0, \qquad \mathrm{NS5B{:}dstiRNA} \xrightarrow{k_{degvms}} 0,$$
$$\mathrm{NS3/4A} \xrightarrow{k_{degns}} 0, \qquad \mathrm{NS5A} \xrightarrow{k_{degns}} 0,$$
$$\mathrm{NS5B}^{\mathrm{cyt}} \xrightarrow{k_{degns}} 0, \qquad \mathrm{NS5B}^{\mathrm{VMS}} \xrightarrow{k_{degvms}} 0,$$
$$\mathrm{Cp} \xrightarrow{k_{degs}} 0.$$

4.2 Parameter values

We use parameter values that have been reported in Aunins *et al.* [4] and are presented in Table 1.

Table 1. Table of parameters values

Parameter	Value	Parameter	Value
k_{tc}	1 molecule^{-1} h^{-1}	k_{trans}	180 h^{-1}
$k_{cleavage}$	9 h^{-1}	k_{hfc}	0.0008 molecule^{-1} h^{-1}
k_{rp5b}	0.1 molecule^{-1} h^{-1}	k_{rip}	0.6 molecule^{-1} h^{-1}
k_{init}	1.12 h^{-1}	k_{rids}	10 molecule^{-1} h^{-1}
k_{repl}	1.12 h^{-1}	k_{outrp}	0.307 h^{-1}
$k_{assembly}$	1.2×10^{-7} molecule^{-1} h^{-1}	k_{degrp}	0.26 h^{-1}
k_{degns}	0.11 h^{-1}	k_{degvms}	0.001 h^{-1}
Rib	5000 molecules	HF	30 molecules
k_{degs}	0.61 h^{-1} from 0 to 21 h, and 0.1 h^{-1} from 21 h onward		

DATA AVAILABILITY

All data generated or analysed during this study are included in this published article.

ACKNOWLEDGEMENTS

PGS and RT thank the Wellcome Trust for financial support through the Joint Investigator Award (110145 & 110146), which also provided funding for P-PD and FF. Moreover, RT thanks the EPSRC for an Established Career Fellowship (EP/R023204/1) and the Royal Society for a Royal Society Wolfson Fellowship (RSWF/R1/180009).

AUTHOR CONTRIBUTIONS STATEMENT

R.T., P.-P.D., and P.G.S. conceived the goals of the study. F.F. and R.J.B. conducted the analysis. F.F., R.J.B., R.T., and P.-P.D. analysed the results. All authors reviewed the manuscript.

COMPETING INTERESTS

The authors declare no conflict of interest.

REFERENCES

[1] J. Abrahão, L. Silva, L. S. Silva, J. Y. B. Khalil, R. Rodrigues, T. Arantes, F. Assis, P. Boratto, M. Andrade, E. G. Kroon, et al. Tailed giant Tupanvirus possesses the most complete translational apparatus of the known virosphere. *Nat. Commun.*, 9(1):749, 2018.

[2] R. Andino, Y. Shirogane, E. Rousseau, J. Voznica, Y. Xiao, W. Su, A. Catching, Z. J. Whitfiled, I. M. Rouzine, and S. Bianco. Experimental and mathematical insights on the interactions between poliovirus and a defective interfering genome. Preprint at `https://www.biorxiv.org/content/10.1101/2021.01.11.426198v1` (2021).

[3] J. Ashley, B. Cordy, D. Lucia, L. G. Fradkin, V. Budnik, and T. Thomson. Retrovirus-like Gag protein Arc1 binds RNA and traffics across synaptic boutons. *Cell*, 172(1):262–274, 2018.

[4] T. R. Aunins, K. A. Marsh, G. Subramanya, S. L. Uprichard, A. S. Perelson, and A. Chatterjee. Intracellular hepatitis C virus modeling predicts infection dynamics and viral protein mechanisms. *J. Virol.*, 92(11), 2018.

[5] C. R. M. Bangham and T. B. L. Kirkwood. Defective interfering particles: effects in modulating virus growth and persistence. *Virology*, 179(2):821–826, 1990.

[6] R. J. Bingham, E. C. Dykeman, and R. Twarock. RNA virus evolution via a quasispecies-based model reveals a drug target with a high barrier to resistance. *Viruses*, 9(11):347, 2017.

[7] G. Cornelis, C. Vernochet, Q. Carradec, S. Souquere, B. Mulot, F. Catzeflis, M. A. Nilsson, B. R. Menzies, M. B. Renfree, G. Pierron, et al. Retroviral envelope gene captures and syncytin exaptation for placentation in marsupials. *Proc. Natl. Acad. Sci.*, 112(5):E487–E496, 2015.

[8] G. Cornelis, M. Funk, C. Vernochet, F. Leal, O. A. Tarazona, G. Meurice, O. Heidmann, A. Dupressoir, A. Miralles, M. P. Ramirez-Pinilla, et al. An endogenous retroviral envelope syncytin and its cognate receptor identified in the viviparous placental Mabuya lizard. *Proc. Natl. Acad. Sci.*, 114(51): E10991–E11000, 2017.

[9] P. Czuppon, F. Débarre, A. Gonçalves, O. Tenaillon, A. S. Perelson, J. Guedj, and F. Blanquart. Success of prophylactic antiviral therapy for SARS-CoV-2: Predicted critical efficacies and impact of different drug-specific mechanisms of action. *PLoS Comput. Biol.*, 17(3):e1008752, 2021.

[10] H. Dahari, J. E. Layden-Almer, E. Kallwitz, R. M. Ribeiro, S. J. Cotler, T. J. Layden, and A. S. Perelson. A mathematical model of hepatitis C virus dynamics in patients with high baseline viral loads or advanced liver disease. *Gastroenterology*, 136(4):1402–1409, 2009.

[11] J. Denner. Function of a retroviral envelope protein in the placenta of a viviparous lizard. *Proc. Natl. Acad. Sci.*, 114(51):13315–13317, 2017.

[12] N. Dimmock. Cloned defective interfering influenza A virus, May 7 2013. US Patent 8,435,508.

[13] N. Dimmock. Method of preventing or treating influenza A viral infection using cloned DI influenza A viral particles, July 28 2015. US Patent 9,089,516.

[14] N. Dimmock and A. Easton. Anti-viral protection with viruses containing defective genome segments, Apr. 8 2014. US Patent 8,691,215.

[15] N. J. Dimmock and A. J. Easton. Defective interfering influenza virus RNAs: time to reevaluate their clinical potential as broad-spectrum antivirals? *J. Virol.*, 88(10):5217–5227, 2014.

[16] N. J. Dimmock, B. K. Dove, P. D. Scott, B. Meng, I. Taylor, L. Cheung, B. Hallis, A. C. Marriott, M. W. Carroll, and A. J. Easton. Cloned defective interfering influenza virus protects ferrets from pandemic 2009 influenza A virus and allows protective immunity to be established. *PLoS ONE*, 7 (12):e49394, 2012.

[17] A. W. Duncan, C. Dorrell, and M. Grompe. Stem cells and liver regeneration. *Gastroenterology*, 137 (2):466–481, 2009.

[18] E. C. Dykeman, P. G. Stockley, and R. Twarock. Packaging signals in two single-stranded RNA viruses imply a conserved assembly mechanism and geometry of the packaged genome. *J. Mol. Biol.*, 425(17):3235–3249, 2013.

[19] E. C. Dykeman, P. G. Stockley, and R. Twarock. Solving a Levinthal's paradox for virus assembly identifies a unique antiviral strategy. *Proc. Natl. Acad. Sci.*, 111(14):5361–5366, 2014.

[20] A. J. Easton, P. D. Scott, N. L. Edworthy, B. Meng, A. C. Marriott, and N. J. Dimmock. A novel

broad-spectrum treatment for respiratory virus infections: influenza-based defective interfering virus provides protection against pneumovirus infection in vivo. *Vaccine*, 29(15):2777–2784, 2011.

[21] F. Fatehi, R. J. Bingham, E. C. Dykeman, N. Patel, P. G. Stockley, and R. Twarock. An intracellular model of hepatitis B viral infection: An in silico platform for comparing therapeutic strategies. *Viruses*, 13(1):11, 2021.

[22] F. Fatehi, R. J. Bingham, E. C. Dykeman, P. G. Stockley, and R. Twarock. Comparing antiviral strategies against COVID-19 via multiscale within-host modelling. *R. Soc. Open Sci.*, 8:210082, 2021.

[23] D. T. Gillespie. Exact stochastic simulation of coupled chemical reactions. *J. Phys. Chem.*, 81(25): 2340–2361, 1977.

[24] E. J. Grow, R. A. Flynn, S. L. Chavez, N. L. Bayless, M. Wossidlo, D. J. Wesche, L. Martin, C. B. Ware, C. A. Blish, H. Y. Chang, et al. Intrinsic retroviral reactivation in human preimplantation embryos and pluripotent cells. *Nature*, 522(7555):221, 2015.

[25] A. S. Huang and D. Baltimore. Defective viral particles and viral disease processes. *Nature*, 226 (5243):325–327, 1970.

[26] T. B. L. Kirkwood and C. R. M. Bangham. Cycles, chaos, and evolution in virus cultures: a model of defective interfering particles. *Proc. Natl. Acad. Sci.*, 91(18):8685–8689, 1994.

[27] D. Li and J. Aaskov. Sub-genomic RNA of defective interfering (D.I.) Dengue viral particles is replicated in the same manner as full length genomes. *Virology*, 468:248–255, 2014.

[28] D. Li, M.-H. Lin, D. J. Rawle, H. Jin, Z. Wu, L. Wang, M. Lor, M. Hussain, J. Aaskov, and D. Harrich. Dengue virus-free defective interfering particles have potent and broad anti-dengue virus activity. *Commun. Biol.*, 4(1):557, 2021.

[29] Y. J. Lin and M. M. Lai. Deletion mapping of a mouse hepatitis virus defective interfering RNA reveals the requirement of an internal and discontiguous sequence for replication. *J. Virol.*, 67(10): 6110–6118, 1993.

[30] A. Mann, A. C. Marriott, S. Balasingam, R. Lambkin, J. S. Oxford, and N. J. Dimmock. Interfering vaccine (defective interfering influenza A virus) protects ferrets from influenza, and allows them to develop solid immunity to reinfection. *Vaccine*, 24(20):4290–4296, 2006.

[31] T. B. Manzoni and C. B. López. Defective (interfering) viral genomes re-explored: impact on antiviral immunity and virus persistence. *Future Virol.*, 13(7):493–503, 2018.

[32] A. C. Marriott and N. J. Dimmock. Defective interfering viruses and their potential as antiviral agents. *Rev. Med. Virol.*, 20(1):51–62, 2010.

[33] S. Noble, L. McLain, and N. J. Dimmock. Interfering vaccine: a novel antiviral that converts a potentially virulent infection into one that is subclinical and immunizing. *Vaccine*, 22(23-24): 3018–3025, 2004.

[34] E. D. Pastuzyn, C. E. Day, R. B. Kearns, M. Kyrke-Smith, A. V. Taibi, J. McCormick, N. Yoder, D. M. Belnap, S. Erlendsson, D. R. Morado, et al. The neuronal gene Arc encodes a repurposed retrotransposon Gag protein that mediates intercellular RNA transfer. *Cell*, 172(1):275–288, 2018.

[35] N. Patel, S. J. White, R. F. Thompson, R. J. Bingham, E. U. Weiß, D. P. Maskell, A. Zlotnick, E. C. Dykeman, R. Tuma, R. Twarock, et al. HBV RNA pre-genome encodes specific motifs that mediate interactions with the viral core protein that promote nucleocapsid assembly. *Nat. Microbiol.*, 2:17098, 2017.

[36] N. Patel, E. Wroblewski, G. Leonov, S. E. V. Phillips, R. Tuma, R. Twarock, and P. G. Stockley. Rewriting nature's assembly manual for a ssRNA virus. *Proc. Natl. Acad. Sci.*, 114(46):12255–12260, 2017.

[37] B. d. M. Quintela, J. M. Conway, J. M. Hyman, J. Guedj, R. W. Dos Santos, M. Lobosco, and A. S. Perelson. A new age-structured multiscale model of the hepatitis C virus life-cycle during infection and therapy with direct-acting antiviral agents. *Front. Microbiol.*, 9:601, 2018.

[38] U. Rand, S. Y. Kupke, H. Shkarlet, M. D. Hein, T. Hirsch, P. Marichal-Gallardo, L. Cicin-Sain, U. Reichl, and D. Bruder. Antiviral activity of influenza A virus defective interfering particles against SARS-CoV-2 replication in vitro through stimulation of innate immunity. *Cells*, 10(7):1756, 2021.

[39] L. I. Rast, I. M. Rouzine, G. Rozhnova, L. Bishop, A. D. Weinberger, and L. S. Weinberger. Conflicting selection pressures will constrain viral escape from interfering particles: Principles for designing resistance-proof antivirals. *PLoS Comput. Biol.*, 12(5):e1004799, 2016.

[40] V. V. Rezelj, L. I. Levi, and M. Vignuzzi. The defective component of viral populations. *Curr. Opin.*

Virol., 33:74–80, 2018.

[41] V. V. Rezelj, L. Carrau, F. Merwaiss, L. I. Levi, D. Erazo, Q. D. Tran, A. Henrion-Lacritick, V. Gausson, Y. Suzuki, D. Shengjuler, et al. Defective viral genomes as therapeutic interfering particles against flavivirus infection in mammalian and mosquito hosts. *Nat. Commun.*, 12(1):2290, 2021.

[42] Ó. Rolfsson, S. Middleton, I. W. Manfield, S. J. White, B. Fan, R. Vaughan, N. A. Ranson, E. Dykeman, R. Twarock, J. Ford, et al. Direct evidence for packaging signal-mediated assembly of bacteriophage MS2. *J. Mol. Biol.*, 428(2):431–448, 2016.

[43] S. Shakeel, E. C. Dykeman, S. J. White, A. Ora, J. J. B. Cockburn, S. J. Butcher, P. G. Stockley, and R. Twarock. Genomic RNA folding mediates assembly of human parechovirus. *Nat. Commun.*, 8(1): 5, 2017.

[44] H. Stewart, R. J. Bingham, S. J. White, E. C. Dykeman, C. Zothner, A. K. Tuplin, P. G. Stockley, R. Twarock, and M. Harris. Identification of novel RNA secondary structures within the hepatitis C virus genome reveals a cooperative involvement in genome packaging. *Sci. Rep.*, 6:22952, 2016.

[45] P. G. Stockley, N. A. Ranson, and R. Twarock. A new paradigm for the roles of the genome in ssRNA viruses. *Future Virol.*, 8(6):531–543, 2013.

[46] P. G. Stockley, R. Twarock, S. E. Bakker, A. M. Barker, A. Borodavka, E. Dykeman, R. J. Ford, A. R. Pearson, S. E. V. Phillips, N. A. Ranson, et al. Packaging signals in single-stranded RNA viruses: nature's alternative to a purely electrostatic assembly mechanism. *J. Biol. Phys.*, 39(2):277–287, 2013.

[47] K. A. S. Thompson and J. Yin. Population dynamics of an RNA virus and its defective interfering particles in passage cultures. *Virol. J.*, 7(1):257, 2010.

[48] K. A. S. Thompson, G. A. Rempala, and J. Yin. Multiple-hit inhibition of infection by defective interfering particles. *J. Gen. Virol.*, 90(4):888–899, 2009.

[49] M. Thomson, C. L. White, and N. J. Dimmock. The genomic sequence of defective interfering Semliki Forest virus (SFV) determines its ability to be replicated in mouse brain and to protect against a lethal SFV infection in vivo. *Virology*, 241(2):215–223, 1998.

[50] S. Yao, A. Narayanan, S. A. Majowicz, J. Jose, and M. Archetti. A synthetic defective interfering SARS-CoV-2. *PeerJ*, 9:e11686, 2021.